J Polym Res (2015) 22: 224
DOI 10.1007/s10965-015-0871-7

ORIGINAL PAPER

# Effects of POSS addition on Non-isothermal crystallization and morphology of PVDF

**Johnny N. Martins**[1] · **Otavio Bianchi**[2] · **César H. Wanke**[2] · **Charles Dal Castel**[3] · **Ricardo V. B. Oliveira**[4]

Received: 2 July 2015 / Accepted: 20 October 2015 / Published online: 30 October 2015


**Abstract** The influence of polyhedral oligomericsilsesquioxane (POSS) content on the rheological behavior, non-isothermal crystallization behavior, and on crystal morphology of the poly(vinylidene fluoride) nanocomposites prepared through melt blending were investigated in this work. Rheological analysis showed that the POSS additiondecreased viscosity as compared to pure PVDF and induced a deviation in the liquid-like behavior predict by Einstein Suspension Sphere Law. The addition of POSS into PVDF promoted chances in the crystallization behavior. The crystallization was slower in the nanocomposite with higher POSS content due to the diluent effect of POSS in this system. Small angle X-ray scattering (SAXS) patterns showed a small increasing in the lamellar region of PVDF. The amorphous region increases significantly with POSS addition. The interface between the crystalline and amorphous region remains practically unchanged.

**Keywords** Poly(vinylidene fluoride) · Polyhedral OligomericSilsesquioxane · Nanocomposites · Non-isothermal crystallization · Crystalline structure

✉ Johnny N. Martins
johnny.martins@ufsc.br

[1] Federal University of Santa Catarina – Campus Blumenau (UFSC), R. Pomerode, 710, Blumenau 89065-300, Brazil

[2] Materials Science Graduate Program (PGMAT), University of Caxias do Sul (UCS), R. Francisco Getúlio Vargas 1130, Caxias do Sul 95070-560, Brazil

[3] Department of Chemical Engineering, University of Waterloo, University Ave M, 200, N2L 3G1, Waterloo, Canada

[4] Centre for Advanced 2D Materials and Graphene Research Centre, National University of Singapore, 6 Science Drive 2, Buona Vista District 117546, Singapore

## Introduction

PVDF is an engineering thermoplastic offering excellent thermal and chemical resistance and mechanical strength. It is seldom considered for applications involving high-speed processing, such as injection molding, because it is a high-melting and slow-crystallizing polymer [1–3]. PVDF exists in at least four main crystalline structures: α-, β-, γ-, and δ - crystal forms. They are distinguished by the conformation of the C-C bond along the chain backbone [4, 5].

Polyhedral oligomeric silsesquioxane (POSS), a hybrid (organic–inorganic) nanostructured chemical, has been used since early 2000's for the preparation of hybrid materials and polymer matrix nanocomposites [6–8]. POSS molecules are cage-like structures described by the general chemical structure $R(SiO_{3/2})_n$, where $n$ indicates the number of silicon atoms($n$ = 8, 10 or 12) [9]. This cage is surrounded by a corona of functional organic groups and it may be a fully condensed "closed" or an "open" structure [9–11].The incorporation of POSS molecules into polymer materials may result in enhancements in macroscopic properties such as increasing of temperature of usage, mechanical properties, and easy of melt state processing [12, 13].

There are a few studies in literature regarding the incorporation of POSS into PVDF. In one of them Monticelli et al. studied the grafting reaction of amino-containing POSS onto the surface of modified PVDF. The authors used this new hybrid material as a selective membrane [14]. Zeng and co-workers [15] performed a simulation study about the miscibility of binary mixtures of PVDF and six different types of POSS. The authors used Monte Carlo Simulation approach for calculation of mixing energies, Flory–Huggins parameter and Gibbs free energy of mixing.

Martins and co-workers [16] prepared PVDF/POSS nanocomposites through melt blending. They studied the influence of a POSS with methacrylate radicals on the morphological,

viscoelastic and thermal properties of PVDF. The POSS changed the PVDF morphology and microstructure of pure polymer. These changes reflected in the macroscopic properties, mainly, in viscoelastic behavior. The addition of POSS into PVDF also induced the formation of two different crystalline phases and increased the degree of crystallinity with the POSS content. Liu et al. [17] prepared a nanocomposite of PVDF and trifluoropropyllsobutyl POSS (FPB-POSS) using solvent evaporation method. They studied the morphology, crystallization, and thermal properties of this system. The addition of POSS induced the formation of larger particles of PVDF chains. Additionally POSS promoted the formation of higher β crystalline phase on PVDF. Also FPB-POSS acted as nanofiller leading to an improvement in mechanical properties, including hardness and elastic property. Liu and coworkers [18] conducted a study regarding the morphology, crystallization, thermal and mechanical properties of PVDF/Fluoropropyl POSS (FP-POSS) nanocomposites. FP-POSS exhibited miscibility with PVDF, enhancing its crystallinity and the thermal degradation of PVDF was not significantly affected by FP-POSS. The authors also reported that FP-POSS, led to remarkable improvement in mechanical properties. The maximum of mechanical properties improvement was achieved at 3 wt.% of FP-POSS.

When PVDF is blended with poly(methyl methacrylate) (PMMA) there is an amorphization effect in the PVDF by the addition of high PMMA contents. Decreased melt temperature for the system is also observed [19]. The addition of an amorphous polymer to a semi-crystalline one generally modifies the crystallinity of the latter, at least when their amorphous phases are miscible [20]. The decrease in melting point of the PVDF resulting from incorporation of PMMA has been reported in literature [21, 22], and was attributed to the favorable interactions of semi-crystalline PVDF with amorphous PMMA. Another effect observed in this system is the decreasing of crystallization peak temperature ($T_c$) and crystallization enthalpy ($\Delta H_c$). According to previous studies, the decreasing of $T_c$ of PVDF when blended with PMMA can be attributed to intermolecular interactions between the carbonyl group of PMMAand the hydrogen of PVDF [22, 23]. The interactions in PVDF/PMMA and PVDF/*methacrylate* POSS are different than the ones found in PVDF/FP-POSS nanocomposites [17, 18].

The addition of small particles into polymer causes different effects depending on the nature of the particle. One of these effects is the deviation in liquid-like behavior predict by Einstein Suspension Sphere Law [24]. Another effect is that small particles have the ability to act as nucleating agents in polymer systems. This trend influences the crystalline morphology by either hindering or facilitating the host polymer crystallization process [25]. The presence of organic radicals in POSS cages interferes in the crystallization process. Moreover, POSS have a different behavior when compared to small particles due to its supramolecular nature. Previous studies have shown that POSS structure remains in the liquid state in the temperature range in which the polymer crystallizes [26].

It is known from previous studies [16–18] that the addition of POSS into PVDF induces a change in polymer morphology, formation of β crystalline phase and improvement of mechanical properties. Nevertheless, the influence of POSS on the crystallization kinetics under non-isothermal conditions, the rheological behavior, and the crystal morphology remains unclear for this nanocomposite.

The aim of this work is to investigate the deviation of the Einstein Suspension Sphere Law caused by addition of POSS into PVDF through melt blending. This deviation effects are correlated with the non-isothermal crystallization kinetics, and crystal morphology of the PVDF.

## Experimental

### Materials

PVDF (Solef 6008, specific mass 1.78 $g.cm^{-3}$, melt flow index 8 $g.10\ min^{-1}$) used in this work was kindly supplied by APTA Resinas Thermoplastics in the pellet form. Liquid POSS was purchased from Hybrid Plastics Inc. The POSS used in this work contain methacryloxypropyl-groups, commercially named *MethacrylPOSS cage mixture* (cod. MA 0735, specific mass 1.20 $g.cm^{-3}$).

### Melt processing

The nanocomposites were prepared through melt blending in a batch mixer (Haake, Rheomix 600p). The experiments were done at 200 °C, 200 rpm for 10 min. This experimental condition makes it possible to approach the steady-state for all compositions under experimental conditions. The POSS content added to PVDF was 0, 1, and 5 wt.%.

### Rheological measurements

The flow curves were obtained in an Anton Parr MCR 101 rheometer using cone plate geometry at 200 °C under nitrogen atmosphere. The dynamic viscosity values were obtained in the shear rate range between $10^{-2}$and $10^{2}s^{-1}$. The rheological parameters were estimated by Cross Model in the range of initial Newtonian viscosities (Eq. 1). The solution of Cross Model was accomplished using non-linear least-squares Levenberg–Marquardt algorithm [27].

$$\eta = \frac{\eta_0}{1 + |\lambda\gamma|^m} \tag{1}$$

Where $\eta_0$ is the zero shear viscosity, $\lambda$ is the time constant and $m$ is a constant factor.

### Differential scanning calorimetry (DSC)

DSC curves were obtained in a TA Instruments Q 2000 under nitrogen atmosphere (samples mass of 9 to 10 mg and flow rate of 50 mL.min$^{-1}$). The melting temperature and enthalpy were calibrated with indium and zinc ($T_{mindium}$ = 156.6 °C; $\Delta H_{indium}$ = 28.47 J.g$^{-1}$). The samples were heated at 40 °C.min$^{-1}$to 220 °C followed by a 5 min isotherm, then cooled to room temperature at different constant cooling rates (5, 10, 15, and 20 °C.min$^{-1}$). The heat flow evolving during the crystallization was recorded as a function of time or temperature. The crystallization enthalpy ($\Delta H_c$) of the crystallized fraction was calculated from the area of the DSC exothermal event.

### Synchrotron small-angle X-ray scattering (SAXS)

The small-angle X-ray scattering experiments were done using the beam line, SAXS1 of the National Synchrotron Light Laboratory (LNLS) in Campinas, Brazil. The SAXS measurements were performed at room temperature in transmission geometry with λ = 1.488 Å. The 2D SAXS spectra were monitored with a photomultiplier and detected on a marCCD 165 detector (8 × 8 binning) with sample-to-detector distance of 602 mm. Samples were placed with their surfaces perpendicular to the direction of the X-ray beam propagation and parallel to the X-ray detector. Samples, with dimensions of 10 × 10 × 3.2 mm$^3$, were cut from the injection molded specimens with controlled cooling. Scattering intensity ($I$) as a function of scattering vectors ($q$) from 0.12 to2.45 nm$^{-1}$was measured. Background and parasitic scattering were determined using an empty holder and subtracted from each measurement.

The X-ray scattering was experimentally determined as a function of the scattering vector ($q$) whose modulus is given by the following Eq.(2):

$$q = \frac{4\pi \sin\theta}{\lambda} \tag{2}$$

Where$\theta$ is half the scattering angle ($2\theta$).

This study considered that the scattering objects are periodical stacks consisting of alternate lamellar crystals and amorphous layers. The detailed parameters of lamellar structures, such as long period ($L_p$), thickness of amorphous layers ($L_a$), and thickness of crystalline layers ($L_c$), can be extracted from SAXS profiles by one-dimensional correlation function, $\gamma$ ($r$) [28–30].

Linear correlation function was determined according to the procedure described in the literature [31] using Lorentz-correction SAXS intensity profiles according to the following equation:

$$\gamma(r) = \frac{\int_0^\infty I(q)q^2\cos(qr)dq}{\int_0^\infty q^2 I(q)dq} = \frac{1}{Q}\int_0^\infty q^2 I(q)\cos(qr)dq \tag{3}$$

Where $r$ is the direction perpendicular to the surfaces of the lamellae, along which the electron density is measured. $Q$ is the invariant that represents the electron density difference between the two phases and it is calculated from the area under the Lorentz-corrected scattering curve. The Porod's law can be used to describe the asymptotic behavior of the background-subtracted SAXS curves at the large $q$ region in the case of an ideal two-phase model with sharp boundaries at the crystal/amorphous interface [32].

The lamellar structure parameters can be determined from the $\gamma(r)$ function [33]. The average crystalline thickness, $Lc$ can be obtained by the intersection of straight line $d\gamma\frac{(r)}{dr}$ with the baseline at $\gamma_{min}$ = - $A$. This baseline is defined as the horizontal tangent at the first $\gamma(r)$ minimum, which belongs to the self-correlation triangle. The volume crystallinity, $\chi_v = \frac{A}{A+\gamma_{max}}$, is defined as a relation between $A$ and $\gamma_{max}$. The $\gamma_{max}$ values is obtained by extrapolation to $r$ = 0 of the straight line $d\gamma\frac{(r)}{dr}$ [29, 33, 34].

The long period, $Lp$, correspond to the $r$ value that belongs to the first $\gamma(r)$ maximum outside the self-correlation triangle. The minimal value of the long period, $L_{pmin}$ corresponds to the double of the $r$ value that belongs to the first $\gamma(r)$ minimum [34]. The average soft block (amorphous) thickness is simply deduced by $L_a = L_{pmin} - L_c$. and the local crystallinity is given by $\chi_L = \frac{L_c}{L_{pmin}}$. The linear correlation analysis permits estimation of the average interface thickness between crystalline and amorphous phases using the relationship between the crystalline thickness and minimum long period using the following equation $IT = L_c\chi_L = \frac{L_c^2}{L_{pmin}}$ [31, 33, 34].

## Results and discussions

### Rheology properties

The PVDF/POSS nanocomposite flow curves are presented in Fig. 1a. All samples presented Newtonian behavior up to 1 s$^{-1}$. From this shear rate on the samples exhibited shear thinning behavior. The addition of POSS induced a lower viscosity as compared to pure PVDF. This fact is related to a

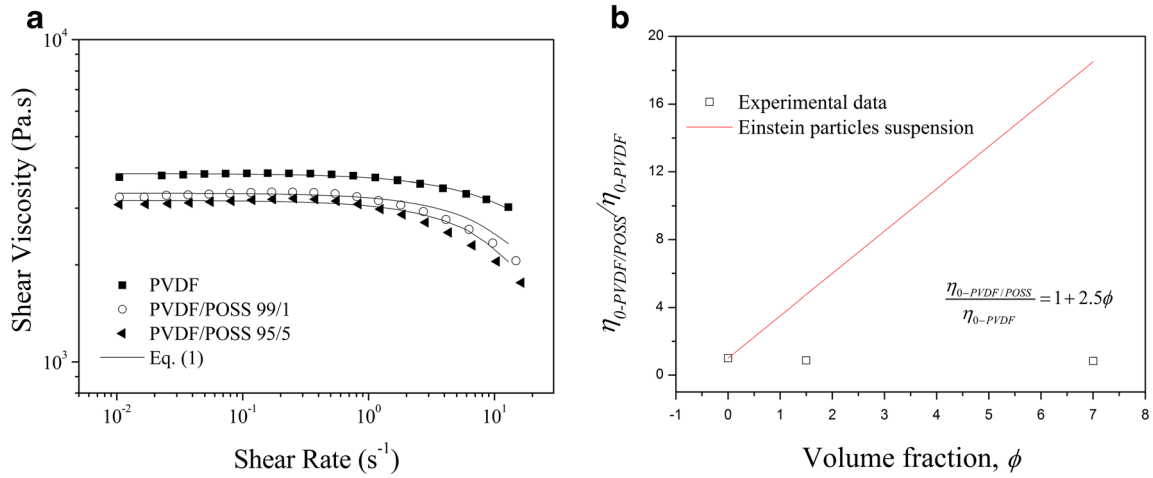


**Fig. 1** a) Flow curves of PVDF/POSS nanocomposites, b) Einstein particles suspensions prediction

lubricant effect, induced by POSS [16].The rheological parameters estimated by Cross Model are summarized in Table 1. For a Newtonian fluid the *m* assume zero values, the *m* values for a pseudoplastic fluid are near 1. The POSS addition caused increasing in *m* and $\lambda$values, which indicates small changing in rheological behavior.

The addition of small particle (d < 10 nm) into a highly viscous liquid induced a decreasing in zero shear viscosity ($\eta_0$) values. The effect of adding small particle in polymer samples causes a deviation in the liquid-like behavior predict by Einstein Suspension Sphere Law. This deviation in Einstein's liquid-like behavior was observed in this PVDF/POSS nanocomposite as showed in Fig. 1b. The POSS structure used in this work has large functional groups methacrylate surrounding the silicon and oxygen structure. POSS structures with functional groups larger than six carbons are generally liquid at room temperature. The fact that POSS particles are small having nanometric scale explains the deviation in the Einstein Suspension Sphere Law in this PVDF/POSS system [16].

## Non-isothermal crystallization

The non-isothermal crystallization curves at various cooling rates as a function of temperature of the PVDF/POSS 100/0, 99/1, and 95/5 are shown in Fig. 2. A dependence of the position and intensity of the exotherms on the cooling rate can be observed. As the cooling rates increases, the crystallization temperature range becomes broader and the peak magnitude higher. As expected, the higher the cooling rates the lower the crystallization peak temperature. Since the crystallization process is time dependent, lower cooling rates give to the macromolecular chains enough time to change conformation. This fact results in a less energetic arrangement, and crystallites are formed at higher temperature.

**Table 1** Rheological parameters obtained by Cross Model for PVDF/POSS nanocomposites

| PVDF/POSS | $\eta_0$ (Pa.s) | $\lambda$ (*s*) | *m* | $R^2$ |
|---|---|---|---|---|
| 100/0 | 3835.8 | 0.02 | 0.88 | 0.987 |
| 99/1 | 3341.1 | 0.04 | 0.98 | 0.987 |
| 95/5 | 3173.5 | 0.05 | 0.98 | 0.981 |

Table 2 presents the non-isothermal crystallization data for pure PVDF and PVDF/POSS nanocomposites obtained at different cooling rates. There was a small increasing in $T_c$ values with the addition of POSS. In the other hand, the melt temperature ($T_m$) was slightly reduced with the addition of POSS. These effects are related to the higher mobility of the polymer chains in the molten state caused by the presence of small particles which reduces the viscosity, as observed in the rheological properties.

There are strong intermolecular interactions between the carbonyl group of PMMA and the hydrogen of PVDF in PVDF/PMMA blends [21, 23, 35–37]. In the same way, PVDF/POSS nanocomposites could also present interactions between the carbonyl groups of methacryl radicals and the acid hydrogen of PVDF. The nanocomposite with 1 wt.% POSS content the processing conditions were efficient to avoid formation of large POSS agglomerates. In the nanocomposites with higher POSS contents these conditions could not be avoid it, because of the strong interaction among POSS molecules [16]. However, the effects on the melt and crystallization behavior are a less noticeable than the ones observed in the polymer blend.

The influence of the POSS content on the dynamic solidification of PVDF/POSS nanocomposites can be monitored through the crystallization rate coefficient (CRC) parameter, proposed by Khanna [38], and Di Lorenzo and Silvestre [39]. As the polymer cools down from the molten state, structures which have symmetrical and short repeating chain segments

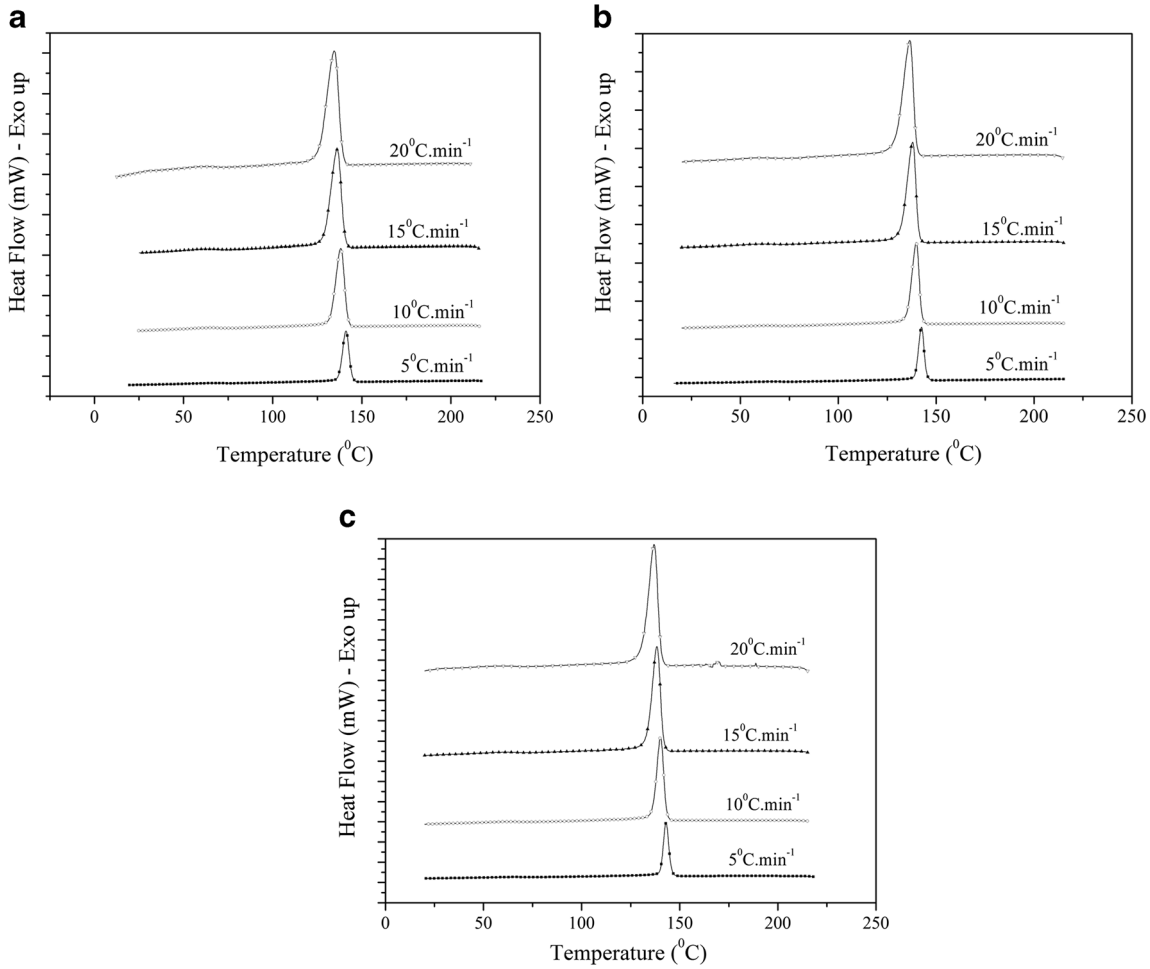


**Fig. 2** The non-isothermal crystallization curves at various cooling rates, a) PVDF/POSS 100/0, b) PVDF/POSS 99/1 and c) PVDF/POSS 95/5

crystallize sooner than those with longer, unsymmetrical, or branched repeating units. In this method, it is considered the cooling rate, $\phi$, dependence on the exothermic peak temperature, $T_c$. It proposes that, once the crystallization begins, it could be hindered by a higher cooling rate. The amount of hindrance would be the least for the fastest crystallizing polymer. By plotting the dependence of $\phi$ against $T_c$, the slope should have a larger absolute value for the polymer with faster crystallization. CRC represents the variation in cooling rate required for a 1 °C change in the undercooling of the polymer melt [38, 39].

Another approach can be done through the use of empirical equations to extract quantitative characteristics from the non-isothermal crystallizations phenomenon [39, 40]. The analysis of the non-isothermal crystallization data can be done in terms of the degree of undercooling$\Delta T_c$, defined as the temperature difference between the temperature at the onset of crystallization, and $T_m$ in the subsequent heating scan. The variation of $\Delta T_c$ with cooling rate,$\phi$, is fitted to the following equation:

$$\Delta T_C = P\phi + \Delta T_c^0 \tag{4}$$

The crystallization rate coefficient (CRC) and degree of undercooling ($\Delta T_c^0$) are presented in Table 3.

**Table 2** $T_m$, $\Delta H_m$, $T_c$, $\Delta H_c$,$X_c$, and $t_{1/2}$forthe non-isothermal crystallization of pure PVDF and PVDF/POSS nanocomposites

| PVDF/POSS | ϕ (°C/min) | $T_m$ (°C) | $\Delta H_m$ (J/g) | $T_c$ (°C) | $\Delta H_c$ (J/g) | $X_c$ (%) | $t_{1/2}$ (s) |
|---|---|---|---|---|---|---|---|
| 100/0 | 5 | 173.7 | 58.2 | 141.1 | 58.8 | 56 | 75 |
| | 10 | 173.1 | 56.4 | 138.2 | 57.7 | 54 | 36 |
| | 15 | 173.1 | 56.2 | 136.1 | 56.5 | 54 | 27 |
| | 20 | 173.2 | 55.5 | 134.5 | 56.5 | 53 | 25 |
| 99/1 | 5 | 172.3 | 59.3 | 142.5 | 59.3 | 57 | 54 |
| | 10 | 172.4 | 58.1 | 139.8 | 58.3 | 56 | 29 |
| | 15 | 172.7 | 57.9 | 137.8 | 56.8 | 56 | 22 |
| | 20 | 172.9 | 55.9 | 136.5 | 55.9 | 54 | 18 |
| 95/5 | 5 | 171.9 | 58.7 | 143.0 | 58.5 | 59 | 58 |
| | 10 | 172.0 | 57.4 | 140.2 | 57.5 | 58 | 30 |
| | 15 | 172.1 | 56.1 | 138.2 | 56.5 | 56 | 22 |
| | 20 | 172.1 | 55.5 | 136.8 | 55.8 | 56 | 19 |

According to the data presented in Table 3, it can be seen that the crystallization rate coefficient (CRC) remained the same for the pure PVDF and the nanocomposite with 1 wt.% POSS. For the nanocomposite with 5 wt.% POSS content there was a decrease of the CRC value. This trend indicates that the crystallization is slower in this material than the other nanocomposites. This fact is related to the diluent effect of POSS in this system. The POSS is in liquid state at the crystallization temperature, so it separates the PVDF chains, interfering in the crystallization process. The degree of under cooling ($\Delta T_c^0$) for the POSS nanocomposites is lower when compared to the pure PVDF. This indicates that the driving force for crystallization of PVDF/POSS nanocomposites is higher than the pure PVDF. The addition of POSS into PVDF promoted chances in the crystallization behavior.

The relative crystallinity,$X_T$, for all samples as a function of temperature were calculated using the expression given in Eq. (5) [41].

$$X_T = \frac{\int_{T_0}^{T} \left(\frac{dH_c}{dT}\right) dT}{\int_{T_0}^{T_\infty} \left(\frac{dH_c}{dT}\right) dT} \tag{5}$$

where$\frac{dH_c}{dT}$ denotes the measured enthalpy of crystallization during an infinitesimal temperature interval $dT$. The limit$T_0$ denotes the initial crystallization temperature and $T_\infty$ is the temperature after the overall crystallization process. Fig. 3 shows the development of relative crystallinity $X_T$ with temperature ($T$) at different cooling rates for PVDF and PVDF/POSS nanocomposites.

All the curves have similar sigmoidal shapes. The curvatures of the lower and upper parts are due to the formation of nuclei and the spherulitic impingement in the early and late stages of crystallization, respectively. It is possible to see that for all materials the curves shifted to the left with an increase in the cooling rate. These curves are typical of a crystallization process, where an induction period is followed by a fast regime that slows down during the late stage.

**Table 3** Crystallization ratecoefficient (CRC) and degree of under cooling ($\Delta T_c^0$) for pure PVDF and PVDF/POSS nanocomposites

| Sample | Crystallization Rate Coefficient (CRC) ($min^{-1}$) | Degree of under cooling ($\Delta T_c^0$) (°C) |
|---|---|---|
| PVDF/POSS (100/0) | 0.46 | 27.78 |
| PVDF/POSS (99/1) | 0.46 | 25.66 |
| PVDF/POSS (95/5) | 0.40 | 24.78 |

Considering the variation of the peak crystallization temperature with the cooling rate $\varphi$, several mathematical procedures have been proposed in literature [39]for the calculation of activation energy, $\Delta E_a$. Among them, the Kissinger's method [42]has been widely applied. However, Kissinger's method has been formulated for heating experiments and Vyazovkin [43] has demonstrated that dropping the negative sign for $\varphi$ is a mathematically invalid procedure that makes the Kissinger's method inapplicable to the processes occurring on cooling. Another limitation is that this method is applicable only to processes whose kinetics can be adequately represented by a constant value of $E_a$. and the effective activation energy of the melt crystallization strongly varies with temperature [44].Therefore, the differential isoconversional method of Friedman [45]or the advanced integral isoconversional method of Vyazovkin [44] are the most appropriate methods for determining the activation energy during crystallization process. In this work, the Friedman method was used and it is given by Eq. (6) [45]

$$\ln\left(\frac{dX_T}{dt}\right)_{(X_T),i} = C - \frac{\Delta E_{a(X_T)}}{RT_{(X_T),i}} \tag{6}$$

Where $C$ is a constant related to $f(X_T)$ and to the pre-exponential factor ($A$). $dX_T/dt$is the instantaneous crystallization rate as function of time at a given relative crystallinity, $R$ is the gas constant, and $\Delta E_a\ (X_T)$ is the effective activation energy, which presents the activation energy at a stage when the crystallized volume fraction is$X_T$. The local activation energy depends on the activation energies of nucleation and growth [46].By selecting appropriate degrees of crystallinity, the values of $dX_T/dt$ at a specific $X_T$ were correlated to the corresponding crystallization temperature at this $X_T$, e.g.,$T_{(X_T)}$ , $i$ to each heating rate. Plotting the left hand side of Eq. (6) with respect to $1/T_{(X_T)}$ , $i$ a straight line is obtained which slope is equal to $\Delta E_a \frac{(X_T)}{R.}$.

The dependence of effective crystallization activation energy of PVDF and PVDF/POSS nanocomposites on the extent of relative crystallization degree calculated using the Friedman's method is presented in Fig. 4.

Overall the calculated energies are negative and increase with the extend of melt crystallization and decrease in temperature in both PVDF and PVDF/POSS nanocomposites. This indicates that as the crystallization proceeds it was more difficult for the polymer to crystalize. The effective activation energy ($E_a$) is higher for the nanocomposites when compared to the pure PVDF. This fact corroborates with the CRC and $\Delta T_c^0$ results pointing out that the energy barrier for crystallization of PVDF/POSS nanocomposites is higher than the pure PVDF. In this case POSS nanoparticles are acting as a barrier

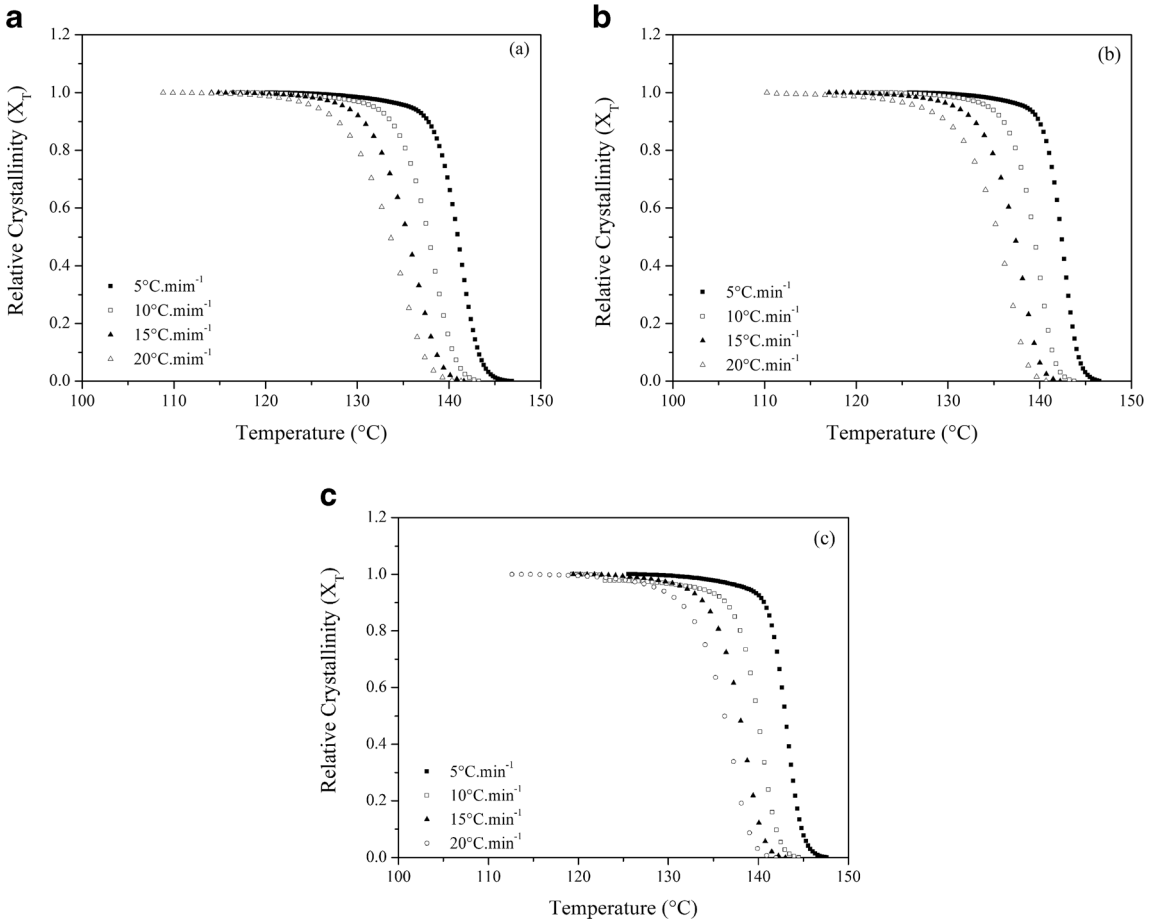


**Fig. 3** Relative Crystallinity as a function of temperature for a) PVDF/POSS 100/0, b) PVDF/POSS 99/1, c) PVDF/POSS 95/5

for molecular diffusion making the crystallization process harder.

Hoffman-Lauritzen equation was modified by Vyazovkin and Sbirrazzuoli so data obtained by DSC during non-isothermal crystallization can be used to calculate the parameters $U^*$ and $K_g$. The Vyazovkin and Sbirrazzuoli Equation is presented below

$$\Delta E_{a(X_T)} = U \times \frac{T_c^2}{(T-T_\infty)^2} + K_g R \frac{\left(T_m^0\right)^2 - T^2 - T_m^0 T}{\left(T_m^0 - T\right)^2 T} \qquad (7)$$

Where $T$ is the average temperature associated with the relative crystallization degree used to calculate, $T_\infty$ is the temperature where diffusion stops, and $T_m{}^0$ represents the equilibrium melting pointing for the polymer. The effective activation energy as a function of average temperature is shown in Fig. 5.

Fig. 5 shows the dependency of effective activation energy on average temperature for PVDF and PVDF/POSS nanocomposites. The experimental calculated data are presented with discrete points while the lines represent the fits of Eq. (7). The fitting showed uniformity between theoretical values and experimental data. The effective activation energy is higher as POSS content increases. The $K_g$ values fitted with Eq. (7) were in the range of $1.59 \times 10^{-6}$ to $2.72 \times 10^{-6}$ $K^2$ and the $U^*$ parameter were in the range of 170 to 352 kJ.mol$^{-1}$. The $K_g$ values increased with POSS addition into PVDF. This trend confirms the assumption that POSS is increasing the energy barrier for crystallization of PVDF.

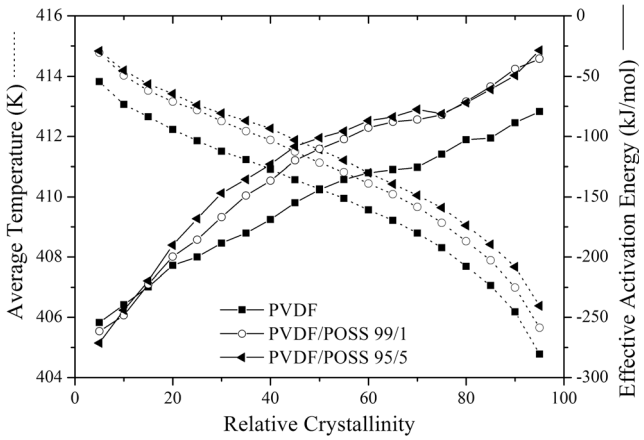


**Fig. 4** Dependence of effective activation energy and average temperature on the extent of relative crystallization for PVDF and PVDF/POSS nanocomposites

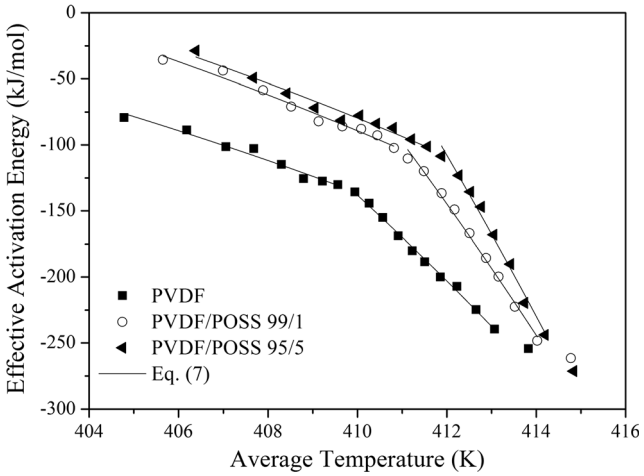


**Fig. 5** Dependence of the effective activation energy on the average temperature for PVDF and PVDF/POSS nanocomposites

## Structural parameters

SAXS is a well-established technique for studying the morphology, shape and size of a multiphase sample, namely aggregates dispersed in liquids, enabling one to obtain structural information on inhomogeneities of the electron density in the samples, with a characteristic length of the order of ten to hundreds of Å [13, 47].

Fig. 6 illustrates the SAXS patterns showing well-defined Bragg peaks around 0.5 $nm^{-1}$. The POSS additionresulted in an increase in scattered intensity in smaller q values than 0.54 $nm^{-1}$. The Bragg peak of the curve with 5 wt.% of POSS was shifted to smaller values of q, which indicates a slight increase in lamellar long period. Fig. 6 (b) shows the curves of the linear correlation function obtained by solving Eq. (3). Addition of POSS results in a small shift to higher *r* values of the first minimum and first maximum. These effects are related to a possible increase in the size of the lamellar structure of the PVDF.

**Table 4** Structural parameters obtained by linear correlation function, γ(r)

| PVDF/ POSS | $L_p$(nm) | $L_a$(nm) | $L_c$ (nm) | $\chi_v$ (%) | $\chi_L$ (%) | *IT* (nm) | *NI* |
|---|---|---|---|---|---|---|---|
| 100/0 | 9.60 | 5.32 | 3.16 | 30 | 37 | 1.18 | 0.014 |
| 99/1 | 10.05 | 5.60 | 3.16 | 29 | 36 | 1.14 | 0.016 |
| 95/5 | 10.70 | 6.20 | 3.40 | 31 | 35 | 1.20 | 0.011 |

The addition of the others components into polymer results in deviations of the two-phase model. In consequence, it is possible to estimate a parameter called non- ideality (*NI*), which is nothing more than a model of the deviation of the lamellar structures. The non-ideality parameter, defined as:

$$NI = \left(\frac{L_p - L_{p\min}}{L_p}\right)^2 \quad (7)$$

In this parameter, a value close to zero means that the system is behaving close to an ideal two-phase model. Table 4 shows values of the structural parameters obtained by applying the two-phase model. The increasing of POSS contents resulted in higher lamellar long period (*Lp*), from 9.6 to 10.7 nm. The thickness of the crystalline region, $L_c$, was less affected than the amorphous thickness, $L_a$. Considering an experimental error of 5 % the $L_c$ values are practically the same, showing that the increasing of *Lp* are more related to the increasing of amorphous thickness. This explains the fact that the Tm and Tc values have small variation. This occurs because the driving force for the crystallization of PVDF is greater than the PVDF-POSS interactions and therefore POSS molecules are segregated into the amorphous regions. The amount of the excluded non-crystalline materials should be altered with time during the spherulite growth due to the change in the concentration at the crystal growth front. During the crystallization process, the change of the exclusion will cause the modification in crystal morphology with the

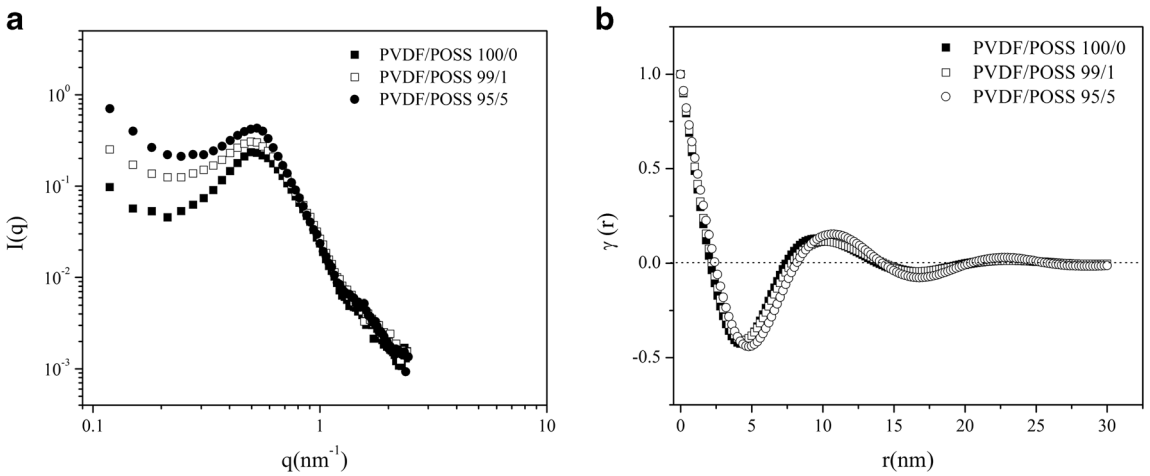


**Fig. 6** SAXS results for PVDF and PVDF/POSS nanocomposites

distance from the center of the spherulite. Regarding the crystallinity of the materials, as can be seen in the DSC results, the addition of POSS hardly affects the values of the crystallization enthalpy; therefore, the SAXS analysis also show no changes in intervals of $\chi_v$ and$\chi_L$ values.

The addition of polymers such as PMMA in PVDFresults in changes in the lamellar structure of the semi-crystalline component. Overall, there was an increasing in the lamellar region of PVDF as the amorphous region increases significantly. Thus the size of the interfacial area between the crystalline and amorphous region increases, which results in a heterogeneous system in the transition region. These changes result in more pronounced deviations in the model and the two-phase increase in non-ideality parameter. For the PVDF/POSS system, the interface between the crystalline and amorphous region is practically unchanged, remaining with values close to the pure PVDF and similar to those found in the literature. Similar behavior is found for the non-ideality parameter.

Thus, due to the small size, the POSS structure is segregated into the amorphous region. This structure contributes to a diluent effect during crystallization of PVDF and therefore causes a decrease in the energy barrier for crystallization. These and other results in the literature suggest that methacrylate POSS has miscibility in the amorphous phase with PVDF.

## Conclusions

The influence of POSS content on the rheological behavior, on the non-isothermal crystallization behavior, and on crystal morphology of the PVDF nanocomposites were evaluated using melt rheology, differential scanning calorimetry and small angle X-Ray scattering. The addition of POSS induced a lower viscosity as compared to pure PVDF, which indicates changing in the rheological behavior. There was a deviation in the liquid-like behavior predict by Einstein Suspension Sphere Law. This was because of POSS particles are small in nanometric range and have methacryloxypropyl-groups which cause this deviation of expected behavior.

PVDF and PVDF/POSS nanocomposites showed similar non-isothermal crystallization data. The small differences in $T_c$ and $T_m$ between pure PVDF and the nanocomposites are related to the higher mobility of the polymer chains in the molten state caused by the presence of small particles, which reduces the viscosity, as observed in the rheological properties. The addition of POSS into PVDF promoted chances in the crystallization behavior. The crystallization was slower in the material with 5 wt.% POSS content. The driving force for crystallization of PVDF/POSS nanocomposites is higher than the pure PVDF due to the diluent effect of POSS in this system. The analysis of Friedman and Hoffman-Lauritzen methods indicated that POSS is increasing the energy barrier for crystallization of PVDF.

The addition of POSS results in small increasing in the amorphous lamellar region of PVDF. The interface between the crystalline and amorphous region is practically unchanged, remaining with values close to the pure PVDF and similar to those found in the literature. Similar behavior is found for the non-ideality parameter. The small deviations of Einstein Suspension Sphere Law caused by POSS were not sufficient to ensure great effects on the non-isothermal crystallization and crystal morphology of PVDF.

**Acknowledgments** The authors are grateful to CNPq, Brazil for financial support (473402/2013-0) and the Brazilian Synchrotron Light Laboratory (LNLS) for the SAXS (SAXS1 beam line) analysis.

## References

1. Chen G-X, Li Y, Shimizu H (2007) Ultrahigh-shear processing for the preparation of polymer/carbon nanotube composites. Carbon 45(12):2334–2340
2. Yee WA, Kotaki M, Liu Y, Lu X (2007) Morphology, polymorphism behavior and molecular orientation of electrospun poly(vinylidene fluoride) fibers. Polymer 48(2):512–521
3. He F, Fan J, Lau S (2008) Thermal, mechanical, and dielectric properties of graphite reinforced poly(vinylidene fluoride) composites. Polym Test 27(8):964–970
4. Danno T, Matsumoto H, Nasir M, Minagawa M, Horibe H, Tanioka A (2009) PVDF/PMMA composite nanofiber fabricated by electrospray deposition: crystallization of PVDF induced by solvent extraction of PMMA component. J Appl Polym Sci 112(4):1868–1872
5. Benz M, Euler WB, Gregory OJ (2002) The role of solution phase water on the deposition of thin films of poly(vinylidene fluoride). Macromolecules 35(7):2682–2688
6. H-x Z, Lee H-y, Y-j S, K-b Y, Noh S-K, Lee D-h (2008) Preparation and characterization of styrene/styryl–polyhedral oligomeric silsesquioxane hybrid copolymers. Polym Int 57(12):1351–1356
7. Sheikh FA, Barakat NAM, Kim B-S, Aryal S, Khil M-S, Kim H-Y (2009) Self-assembled amphiphilic polyhedral oligosilsesquioxane (POSS) grafted poly(vinyl alcohol) (PVA) nanoparticles. Mater Sci Eng C 29(3):869–876
8. De Nardi MJ, Bof de Oliveira RV (2013) Estabilidade térmica de nanocompósitos de poli(fluoreto de vinilideno) e POSS. Scientia cum Industria 1(1):1–5
9. Luvison C, Farias MCM, Bianchi O (2014) Modificação química de nanoestruturas híbridas (POSS) Para aplicação Como lubrificantes. Scientia cum Industria 2(1):19–25
10. Joshi M, Butola BS, Simon G, Kukaleva N (2006) Rheological and viscoelastic behavior of HDPE/octamethyl-POSS nanocomposites. Macromolecules 39(5):1839–1849
11. Sánchez-Soto M, Schiraldi DA, Illescas S (2009) Study of the morphology and properties of melt-mixed polycarbonate–POSS nanocomposites. Eur Polym J 45(2):341–352
12. Zheng L, Waddon AJ, Farris RJ, Coughlin EB (2002) X-ray characterizations of polyethylene polyhedral oligomeric silsesquioxane copolymers. Macromolecules 35(6):2375–2379
13. Bianchi O, Barbosa LG, Machado G, Canto LB, Mauler RS, Oliveira RVB (2013) Reactive melt blending of PS-POSS hybrid nanocomposites. J Appl Polym Sci 128(1):811–827

14. Monticelli O, Waghmare P, Chincarini A (2009) On the preparation and application of novel PVDF–POSS systems. J Mater Sci 44(7): 1764–1771
15. Fan-lin Z, Yi S, Yu Z, Qing-kun L (2011) A molecular dynamics simulation study to investigate the elastic properties of PVDF and POSS nanocomposites. Model Simul Mater Sci Eng 19(2):025005
16. Martins JN, Bassani TS, Oliveira RVB (2012) Morphological, viscoelastic and thermal properties of poly(vinylidene fluoride)/POSS nanocomposites. Mater Sci Eng C 32(2):146–151
17. Liu Y, Sun Y, Zeng F, Chen Y, Li Q, Yu B, Liu W (2013) Morphology, crystallization, thermal, and mechanical properties of poly(vinylidene fluoride) films filled with different concentrations of polyhedral oligomeric silsesquioxane. Polym Eng Sci 53(7):1364–1373
18. Liu Y, Sun Y, Zeng F, Liu J, Ge J (2013) Effect of POSS nanofiller on structure, thermal and mechanical properties of PVDF matrix. J Nanoparticle Res 15(12):1–10
19. Ray S, Easteal AJ, Cooney RP, Edmonds NR (2009) Structure and properties of melt-processed PVDF/PMMA/polyaniline blends. Mater Chem Phys 113(2–3):829–838
20. Long Y, Shanks RA, Stachurski ZH (1995) Kinetics of polymer crystallisation. Prog Polym Sci 20(4):651–701
21. Freire E, Bianchi O, Forte MMC, Preto M, Monteiro EEC, Tavares MIB (2008) Thermal and low-field NMR study on poly(vinylidene fluoride) and their physical mixtures with poly(methyl methacrylate). Polym Eng Sci 48(10):1901–1909
22. Freire E, Bianchi O, Martins JN, Monteiro EEC, Forte MMC (2012) Non-isothermal crystallization of PVDF/PMMA blends processed in low and high shear mixers. J Non-Cryst Sol 358(18–19):2674–2681
23. Okabe Y, Murakami H, Osaka N, Saito H, Inoue T (2010) Morphology development and exclusion of noncrystalline polymer during crystallization in PVDF/PMMA blends. Polymer 51(6): 1494–1500
24. Einstein A (1905) Über die von der molekularkinetischen theorie der wärme geforderte bewegung von in ruhenden flüssigkeiten suspendierten teilchen. Ann Phys 322(8):549–560
25. Ferreira CI, Dal Castel C, Oviedo MAS, Mauler RS (2013) Isothermal and non-isothermal crystallization kinetics of polypropylene/exfoliated graphite nanocomposites. Thermochim Acta 553:40–48
26. Bianchi O, Martins JN, Luvison C, Echeverrigaray SG, Dal Castel C, Oliveira RVB (2014) Melt crystallization kinetics of polyhedral oligomeric silsesquioxane under non-isothermal conditions. J Non-Cryst Sol 394–395:29–35
27. Bates MD, G DW (2007) Regression analysis and its applications. Wiley, Hoboken
28. Albrecht T, Strobl G (1996) Observation of the early stages of crystallization in polyethylene by time-dependent SAXS: transition from individual crystals to stacks of lamellae. Macromolecules 29(2):783–785
29. Sun Y-S (2006) Temperature-resolved SAXS studies of morphological changes in melt-crystallized poly(hexamethylene terephthalate) and its melting upon heating. Polymer 47(23):8032–8043
30. Denchev Z, Nogales A, Ezquerra TA, Fernandes-Nascimento J, Baltà-Calleja FJ (2000) On the origin of the multiple melting behavior in poly(ethylene naphthalene-2,6-dicarboxylate): microstructural study as revealed by differential scanning calorimetry and X-ray scattering. J Polym Sci B Polym Phys 38(9):1167–1182
31. Carli LN, Bianchi O, Machado G, Crespo JS, Mauler RS (2013) Morphological and structural characterization of PHBV/organoclay nanocomposites by small angle X-ray scattering. Mater Sci Eng: C 33(2):932–937
32. Cardoso MB, Westfahl Jr H (2010) On the lamellar width distributions of starch. Carbohydr Polym 81(1):21–28
33. Fatnassi M, Ben Cheikh Larbi F, Halary JL (2010) Quantitative analysis of semicrystalline blends SAXS data: theoretical modeling versus linear correlation function. Int J of Polym Sci 2010:6
34. Fatnassi M, Ben Cheikh Larbi F, Dubault A, Halary JL (2005) Structural study of semi-crystalline blends of poly(vinylidene fluoride) and poly(methyl methacrylate) by means of linear correlation and interface distribution functions. E-Polymers 2005:056
35. Hourston DJ, Hughes ID (1977) Poly(vinylidene fluoride) - poly(methyl methacrylate) blends. Polymer 18(11):1175–1178
36. Leonard C, Halary JL, Monnerie L (1988) Crystallization of poly(vinylidene fluoride)-poly(methyl methacrylate) blends: analysis of the molecular parameters controlling the nature of poly(vinylidene fluoride) crystalline phase. Macromolecules 21(10):2988–2994
37. Freire E, Bianchi O, Monteiro EEC, Reis Nunes RC, Forte MC (2009) Processability of PVDF/PMMA blends studied by torque rheometry. Mater Sci Eng C 29(2):657–661
38. Khanna YP (1990) A barometer of crystallization rates of polymeric materials. Polym Eng Sci 30(24):1615–1619
39. Di Lorenzo ML, Silvestre C (1999) Non-isothermal crystallization of polymers. Prog Polym Sci 24(6):917–950
40. Nadkarni VM, Bulakh NN, Jog JP (1993) Assessing polymer crystallizability from nonisothermal crystallization behavior. Adv Polym Technol 12(1):73–79
41. Papageorgiou GZ, Achilias DS, Bikiaris DN, Karayannidis GP (2005) Crystallization kinetics and nucleation activity of filler in polypropylene/surface-treated SiO2 nanocomposites. Thermo Acta 427(1–2):117–128
42. Kissinger HE (1957) Reaction kinetics in differential thermal analysis. Anal Chem 29(11):1702–1706
43. Vyazovkin S, Sbirrazzuoli N (2003) Estimating the activation energy for non-isothermal crystallization of polymer melts. J Therm Anal Calorim 72(2):681–686
44. Vyazovkin S, Stone J, Sbirrazzuoli N (2005) Hoffman-lauritzen parameters for non-isothermal crystallization of poly(ethylene terephthalate) and poly(ethylene oxide) melts. J Therm Anal Calorim 80(1):177–180
45. Friedman HL (1964) Kinetics of thermal degradation of char-forming plastics from thermogravimetry. Application to a phenolic plastic. J Polym Sci C: Polym Symp 6(1):183–195
46. Lu W, Yan B, W-h H (2005) Complex primary crystallization kinetics of amorphous finemet alloy. J Non-Cryst Sol 351(40–42): 3320–3324
47. Mota AAR, Gatto CC, Machado G, de Oliveira HCB, Fasciotti M, Bianchi O, Eberlin MN, Neto BAD (2014) Structural organization and supramolecular interactions of the task-specific ionic liquid 1-methyl-3-carboxymethylimidazolium chloride: solid, solution, and gas phase structures. J Phys Chem C 118(31):17878–17889